Computer Assisted Mechanics and Engineering Sciences, 5: 421–441, 1998.

Rest-to-rest attitude maneuvers of a satellite with flexible solar panels by using input shapers

Setyamartana Parman and Hideo Koguchi
Department of Mechanical Engineering, Nagaoka University of Technology
Kamitomioka-machi 1603-1, Nagaoka-shi, Niigata, 940-2188 Japan

(Received December 29, 1997)

A hybrid system of coordinates and a relatively general *Lagrangian formulation* for studying the dynamics and control of spacecraft with flexible members is developed. Versatility of the formulation is illustrated through a dynamical study of the satellite with two symmetrical flexible solar panels, where the *finite element method* is used to describe elastic deformations of solar panels modelled as flat plate structures in bending. The performance of the satellite undergoing roll maneuver is simulated. Results indicate that, under an unshaped input, the maneuvers induce undesirable roll motion of the satellite as well as vibration of the solar panels. A *zero vibration input shaper* is then applied to reduce the largest magnitude of residual oscillation of roll motion. Once the shaped roll torque input is applied to the satellite, the performance improves significantly. When the longest distance of impulsing time sequences in the input shaper is close enough to the period of large amplitude vibration of flexible members, its maximum deflection during attitude maneuver will also be close enough to the amplitude of vibration with this period under the bang-bang input.

1. Introduction

Precise orientation of spacecraft during its operation in space needs frequently corrections of its attitude. Attitude maneuver of rigid spacecraft can be done without a lot of vibration problems after reaching its desired attitude. For the flexible spacecraft maneuvering the attitude without regarding to system flexibility or without controls on the flexible members, large amplitude transient and steady-state oscillations may occur, especially when the system is equipped with on-off jets. Such system often needs a rest-to-rest attitude maneuver with limited vibration both during and at the end of the maneuver. For example, it may be necessary to generate a torque profile such that the flexible spacecraft is rotated through a desired attitude angle, while the deflections of flexible members remain small throughout the maneuver and go to zero at the end of the maneuver.

To minimize modal vibration in a flexible satellite system, Swiggert [13] proposed shaped torque commands constructed from the finite trigonometric series. The method is implemented by convolving a sequence of impulses, an input shaper, with a desired system command to produce a shaped input that then is used to drive the system. The amplitudes and time locations of the impulses are determined by solving a set of constraint equations that attempt to control the dynamic response of the system.

A flexible satellite equipped with on-off reaction jets cannot produce the variable-amplitude actuation force that is usually required with input shaping; the satellite must be moved with constant amplitude force pulses. Some heuristic methods for extending input shaping to the case of on-off actuators have been developed by Rogers and Seering [8]. The use of constraint on the impulse amplitudes have been used to generate time-optimal command profiles for on-off reaction jets. Liu and Wie [6], Singh and Vadali [9], Wie, Sinha, and Liu [15] demonstrated on-off input shaping with mass, spring, and damper simulations. These works have been concentrated on eliminating the residual vibration. No constraints were placed on the amplitude of deflection during the slew. Pao and Singhose [7] showed that input shaping is very successful at eliminating residual vibration and

has the benefit of decreasing transient deflection when compared to bang-bang control. However the amplitude of the transient deflection is not limited and still can be very large. It is well known that large structural deflections induce large internal loads, and hence, deflection limiting is very important. Singhose, Banerjee, and Seering [12] studied input shaping to observe slew maneuvers of flexible spacecraft with the limitation on member deflection. They modelled the spacecraft as a spring-mass system, both for rotary system and linear system. Such simple models having one flexible mode and a rigid-body mode, so that the expressions for the deflection of the systems can be derived easily. But for the system observed having a lot of flexible modes, such as the finite element model of satellite with flexible solar panels studied by Koguchi and Parman [3, 4, 5], the derivation of expressions for flexible member's deflections becomes very troublesome.

This paper presents computer simulations of rest-to-rest attitude maneuvers of a satellite with flexible solar panels under shaped roll inputs in a limited duration time. The equations of motion are derived by using a hybrid set of coordinates and Lagrange's formulation, and the finite element method is used to describe elastic deformations of solar panels modelled as flat plate structures in bending, such as the model proposed by Koguchi and Parman [3, 4, 5]. The shaped input is selected to make zero vibration on the frequency with the greatest amplitude of residual attitude oscillation. Based on the results of computer simulations, the influence of shaped input profiles with respect to the maximum deflection of solar panel during attitude maneuver will be studied.

2. Formulation of the Equations of Motion

In order to formulate the equations of motion of a flexible satellite in space a system of reference frames to measure motions of each structural subsystem needs to be determined. Factors that will affect the choice of reference frames are: (i) the simplicity in expressing the potential and kinetic energy functions; (ii) the simplicity in formulating the equations of motion; (iii) the simplicity of constraint equations relating to the orientation of the frame relative to the structural subsystem; and (iv) the ability to separate equations governing the satellite's rigid body motions from the motions of elastic deformations of flexible substructures.

The satellite upon consideration is a gravity oriented-stabilized satellite containing a rigid main body and two symmetrical flexible solar panels, such as the Canadian Communications Technology Satellite in a circular orbit. Environmental drags to the satellite during orbiting the earth are supposed to be absent or can be neglected. As a lot of works in flexible spacecraft dynamics, a hybrid system of coordinates is used in this paper. As discrete coordinates to express unrestricted motions of rigid main body, the inertial reference frame, orbital reference frame, and rigid body-fixed reference frame are defined. As distributed coordinates to describe flexible substructure time-varying deformations the flexible substructure local reference frames are used. The inertial reference frame is a reference frame where all unrestricted dynamic motions of the satellite will be referred to. Its coordinate system is fixed with respect to the stars and guarantees a required accuracy over a time interval of interest. In this paper, in a short time of observation, the inertial reference frame $F_i(O_iX_iY_iZ_i)$ is defined as follows (see Fig. 1): (i) the origin of the inertial reference frame, O_i, is selected at a location of nominal orbit of the satellite, (ii) the first axis, X_i, directed along a fixed celestial direction in the orbit plane, (iii) the second axis, Y_i, is normal to the orbit plane, (iv) and the third axis, Z_i, complete the orthogonal set, i.e. in the orbit plane too. The orbital reference frame, F_o $(O_oX_oY_oZ_o)$, is defined as follows: (i) the origin of the orbital reference frame O_o is located on the nominal satellite orbit, (ii) the first axis, X_o, points to the orbital direction, (iii) the second axis, Y_o, is normal to the orbit plane, (iv) and the third axis, Z_o, points to the centre of earth. The orbital reference frame can be obtained from the inertial reference frame by rotation $\omega_o t + \theta_0$ along Y_i-axis, where ω_o is the orbital angular velocity, and θ_0 is a constant angle (see Fig. 1). The rigid body-fixed reference frame $F_b(O_bX_bY_bZ_b)$ is assumed to be fixed on the rigid main body, and flexible substructure reference frames $F_l(O_lX_lY_lZ_l)$ are assumed to be fixed on each substructure. The orientation of the rigid body-fixed frame relative to the orbital reference frame is

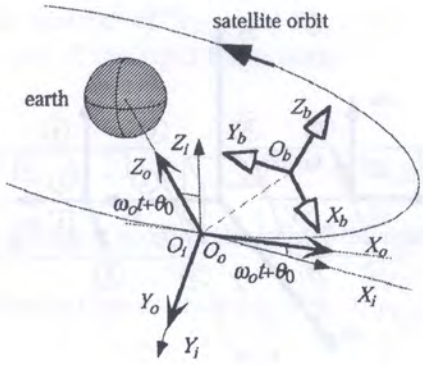

Fig. 1. The inertial reference frame F_i, orbital reference frame F_o, and body-fixed reference frame F_b definitions

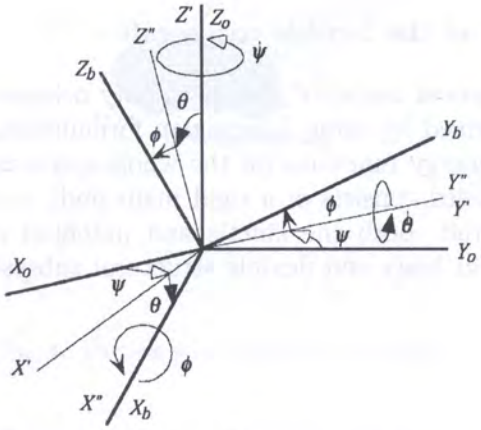

Fig. 2. The transformation from the orbital reference frame F_o to the main body fixed reference frame F_b

expressed in *Bryant's angles*: roll (ϕ), pitch (θ), and yaw (ψ); where the definition of these angles can be seen in Fig. 2. Thus, by seeing Fig. 2, the transformation from F_o to F_b is accomplished by premultiplication with the transformation matrix $\mathbf{T}_{o,b}$, which appears as

$$\mathbf{T}_{o,b} = \begin{bmatrix} c\theta c\psi & c\theta s\psi & -s\theta \\ s\phi s\theta c\psi - c\phi s\psi & s\phi s\theta s\psi + c\phi c\psi & s\phi c\theta \\ c\phi s\theta c\psi + s\phi s\psi & c\phi s\theta s\psi - s\phi c\psi & c\phi c\theta \end{bmatrix} \tag{1}$$

where s and c in the above equation express the sin and cos functions respectively. The rigid body-fixed frame and substructure frames are shown in Fig. 3. All reference frames in this paper are right-hand-side orthogonal system.

The satellite carries two symmetrical flexible solar panels shown in Fig. 3, which longitudinal axis is in the Y_b-axis direction of main body. For the finite element application, each solar panel is divided into 16 rectangular bending plate elements. The elements on the right-hand-side are numbered from 1 until 16 and on the left-hand-side are from 17 until 32, while their nodal points are numbered from 1 until 27 and from 28 until 54. Substructure local reference frames on the left-hand-side $F_l(l = 17, 18, ..., 32)$ have the same normal directions (Z_l-axes) to the solar panel's plane but the reverse in-plane directions (X_l and Y_l-axes) with the frames on the right-hand-side $F_l(l = 1, 2, ..., 16)$. Both the Y_b-axis of rigid body and Y_l-axes of right-hand-side substructure are in the same direction. The origin of rigid body-fixed frame O_b is placed on the midpoint of the longitudinal axis of solar panels. Solar panels are oriented towards the sun, and the declination with respect the X_b-axis of rigid body frame is identified by the offset angle δ.

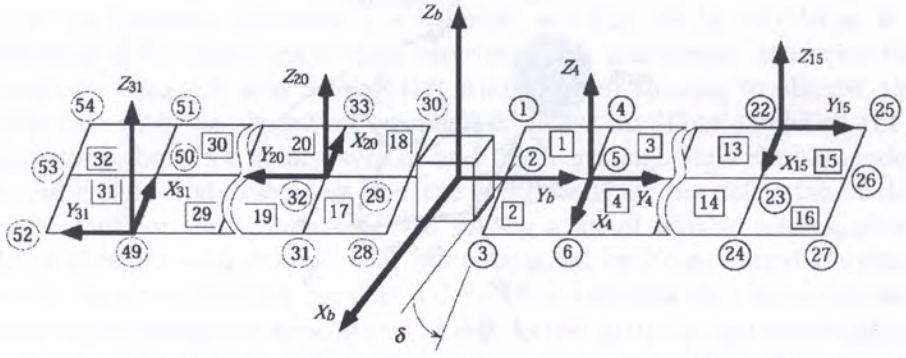

Fig. 3. The model of satellite being investigated; element numbering, nodal point numbering, rigid main body fixed reference frame, and local reference frames

2.1. Equations of motion of the flexible spacecraft

In this section, the mathematical model of general gravity oriented and nonspinning flexible spacecraft dynamics will be derived by using Lagrangian formulation, so that the expressions of kinetic energy and potential energy functions for the whole spacecraft need to be determined first. The spacecraft to be considered consists of a rigid main body and several attached flexible substructures. For such spacecraft, both the kinetic and potential energies can be determined by evaluating the values for rigid body and flexible structural subsystems separately, then summing the results.

2.1.1. Kinetic energy

To formulate the kinetic energy of the spacecraft, we must consider firstly the kinetic energy of a particle p with mass dm relative to the inertial reference frame, which can be written as

$$dE_k = \frac{1}{2}\dot{\mathbf{r}}_{i,p}^T \dot{\mathbf{r}}_{i,p} dm, \tag{2}$$

where $\mathbf{r}_{i,p}$ is a vector from the origin of inertial reference frame O_i to the discussed particle p, and the overdot ($\dot{}$) means differentiation with respect to time relative to the inertial reference frame.

For particle p of the rigid body, $\mathbf{r}_{i,p}$ can be expressed as

$$\mathbf{r}_{i,p} = \mathbf{r}_{i,b} + \mathbf{r}_{b,p}, \tag{3}$$

and $\dot{\mathbf{r}}_{i,p}$ as

$$\dot{\mathbf{r}}_{i,p} = \dot{\mathbf{r}}_{i,b} + \boldsymbol{\omega}_{b,i} \times {}^b\mathbf{r}_{b,p}, \tag{4}$$

where $\mathbf{r}_{i,b}$ is a vector from O_i to O_b, ${}^b\mathbf{r}_{b,p}$ is a vector from O_b to the particle p expressed in F_b, and $\boldsymbol{\omega}_{b,i}$ is the angular velocity vector of F_b relative to F_i. By using Eq. (4), the integration of Eq. (2) will result the kinetic energy of the rigid body of spacecraft in the following form:

$$E_{k_b} = \frac{1}{2}\dot{\mathbf{r}}_{i,b}^T \dot{\mathbf{r}}_{i,b}\, m_b + \frac{1}{2}\boldsymbol{\omega}_{b,i}^T \mathbf{I}_b \boldsymbol{\omega}_{b,i} + \dot{\mathbf{r}}_{i,b}^T \mathbf{Q}_b \boldsymbol{\omega}_{b,i}, \tag{5}$$

where m_b is the mass of the rigid main body, $\mathbf{I}_b$ is the inertia matrix of the main body relative to the origin of the rigid body-fixed frame O_b:

$$\mathbf{I}_b = \int_{m_b} {}^b\tilde{\mathbf{r}}_{b,p}^T \, {}^b\tilde{\mathbf{r}}_{b,p}\, dm \tag{6}$$

since ${}^b\tilde{\mathbf{r}}_{b,p}$ is the skew-symmetric matrix[1] of ${}^b\mathbf{r}_{b,p}$, and $\mathbf{Q}_b$ is the coupling matrix between translational and rotational displacements of the rigid main body:

$$\mathbf{Q}_b = \int_{m_b} {}^b\tilde{\mathbf{r}}_{b,p}^T \, dm. \tag{8}$$

If the origin of rigid body-fixed frame coincides the centre of mass of the main body, the value of $\mathbf{Q}_b$ is equal to zero.

For particle p in a flexible substructure as shown in Fig. 4, $\mathbf{r}_{i,p}$ can be expressed in the following form:

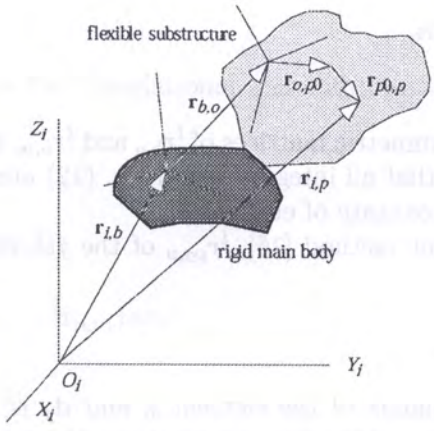

Fig. 4. Particle p in a flexible substructure

$$\mathbf{r}_{i,p} = \mathbf{r}_{i,b} + \mathbf{r}_{b,o} + \mathbf{r}_{o,p_0} + \mathbf{r}_{p_0,p} \tag{9}$$

and $\dot{\mathbf{r}}_{i,p}$ in the following expression:

$$\dot{\mathbf{r}}_{i,p} = \dot{\mathbf{r}}_{i,b} + {}^b\dot{\mathbf{r}}_{b,o} + {}^b\dot{\mathbf{r}}_{p_0,p} + \boldsymbol{\omega}_{b,i} \times ({}^b\mathbf{r}_{b,o} + {}^b\mathbf{r}_{o,p_0} + {}^b\mathbf{r}_{p_0,p}), \tag{10}$$

where $\mathbf{r}_{b,o}$ is a vector from O_b to an origin of flexible substructure local reference frame O_l, $\mathbf{r}_{o,p_0}$ is a vector from O_l to the observed particle p in the undeformed state of substructure, $\mathbf{r}_{p_0,p}$ is the deformation vector of particle p, ${}^b\dot{\mathbf{r}}_{b,o}$ and ${}^b\dot{\mathbf{r}}_{p_0,p}$ are the differentiations of $\mathbf{r}_{b,o}$ and $\mathbf{r}_{p_0,p}$ with respect to time measured in F_b, while ${}^b\mathbf{r}_{b,o}$, ${}^b\mathbf{r}_{o,p_0}$, and ${}^b\mathbf{r}_{p_0,p}$ are $\mathbf{r}_{b,o}$, $\mathbf{r}_{o,p_0}$, and $\mathbf{r}_{p_0,p}$ being expressed in F_b respectively.

The deformation vector of particle p, $\mathbf{r}_{p_0,p}$, for the simplicity in expression and efficiency in numerical calculation, is expressed in the substructure local reference frame. If the orientation of undeformed state of flexible substructures relative to the rigid main body does not vary with respect to time, i.e. the angular velocity of F_l relative to F_b equals to zero, Eq. (10) then can be expressed as

$$\dot{\mathbf{r}}_{i,p} = \dot{\mathbf{r}}_{i,b} + \mathbf{T}_{b,l}^T({}^l\dot{\mathbf{r}}_{b,o} + {}^l\dot{\mathbf{r}}_{p_0,p}) + \boldsymbol{\omega}_{b,i} \times \mathbf{T}_{b,l}^T({}^l\mathbf{r}_{b,o} + {}^l\mathbf{r}_{o,p_0} + {}^l\mathbf{r}_{p_0,p}), \tag{11}$$

where $\mathbf{T}_{b,l}$ is the transformation matrix from F_b to F_l.

[1] A skew-symmetric matrix is an operator to represent the vector product in matrix notation, that is for a vector $\mathbf{r} = \{r_x \; r_y \; r_z\}^T$ the one has

$$\tilde{\mathbf{r}} = \begin{bmatrix} 0 & -r_z & r_y \\ r_z & 0 & -r_x \\ -r_y & r_x & 0 \end{bmatrix} \tag{7}$$

Let us consider that flexible substructures are represented by N elastic elements. Employing Eq. (11)), the integration of Eq. (2) for the element j (j=1, 2, ..., N) of flexible substructure will result

$$\begin{aligned} E_{ka_j} = \; & \frac{1}{2}\dot{\mathbf{r}}_{i,b}^T\dot{\mathbf{r}}_{i,b}m_j + \frac{1}{2}\int_{m_j} {}^l\dot{\mathbf{r}}_{p_0,p}^T\,{}^l\dot{\mathbf{r}}_{p_0,p}dm \\ & + \frac{1}{2}\boldsymbol{\omega}_{b,i}^T\mathbf{T}_{b,l}^T\int_{m_j}({}^l\tilde{\mathbf{r}}_{b,o} + {}^l\tilde{\mathbf{r}}_{o,p_0})^T({}^l\tilde{\mathbf{r}}_{b,o} + {}^l\tilde{\mathbf{r}}_{o,p_0})dm\mathbf{T}_{b,l}\boldsymbol{\omega}_{b,i} \\ & + \boldsymbol{\omega}_{b,i}^T\mathbf{T}_{b,l}^T\int_{m_j}({}^l\tilde{\mathbf{r}}_{b,o} + {}^l\tilde{\mathbf{r}}_{o,p_0})\,{}^l\dot{\mathbf{r}}_{p_0,p}dm + \dot{\mathbf{r}}_{i,b}^T\mathbf{T}_{b,l}^T\int_{m_j}({}^l\tilde{\mathbf{r}}_{b,o} + {}^l\tilde{\mathbf{r}}_{o,p_0})^T dm\mathbf{T}_{b,l}\boldsymbol{\omega}_{b,i} \\ & + \dot{\mathbf{r}}_{i,b}^T\mathbf{T}_{b,l}^T\int_{m_j}{}^l\dot{\mathbf{r}}_{p_0,p}\,dm, \end{aligned} \tag{12}$$

where ${}^l\tilde{\mathbf{r}}_{b,o}$ and ${}^l\tilde{\mathbf{r}}_{o,p_0}$ are skew symmetric matrices of ${}^l\mathbf{r}_{b,o}$ and ${}^l\mathbf{r}_{o,p_0}$ respectively, and m_j is the mass of element j. It should be noted that all integrations in Eq. (12) are extended over the undeformed state which serves as the reference state of element j.

By following the finite element method [16], ${}^l\mathbf{r}_{p_0,p}$ of the jth element can be expressed in the following form:

$${}^l\mathbf{r}_{p_0,p}(x,y,z) = \mathbf{C}_j(x,y,z)\mathbf{d}_j, \tag{13}$$

where $\mathbf{C}_j$ is a shape function matrix of the element j, and $\mathbf{d}_j$ is the displacement vector of the element j. The total kinetic energy of flexible substructures then can be produced in the following form:

$$\begin{aligned} E_{ka} = \; & \sum_{j=1}^{N} E_{ka_j} = \frac{1}{2}\dot{\mathbf{r}}_{i,b}^T\dot{\mathbf{r}}_{i,b}m_a + \frac{1}{2}\dot{\mathbf{d}}^T\mathbf{M}\dot{\mathbf{d}} + \frac{1}{2}\boldsymbol{\omega}_{b,i}^T\mathbf{I}_a\boldsymbol{\omega}_{b,i} \\ & + \boldsymbol{\omega}_{b,i}^T\mathbf{A}\dot{\mathbf{d}} + \dot{\mathbf{r}}_{i,b}^T\mathbf{W}\dot{\mathbf{d}} + \dot{\mathbf{r}}_{i,b}^T\mathbf{Q}_a\boldsymbol{\omega}_{b,i} \end{aligned} \tag{14}$$

where

$$m_a = \sum_{j=1}^{N} m_j \tag{15}$$

is the total mass of flexible substructures,

$$\mathbf{M} = \sum_{j=1}^{N}\mathbf{P}_j^T\mathbf{M}_j\mathbf{P}_j \tag{16}$$

is the total mass matrix of flexible substructures,

$$\mathbf{I}_a = \sum_{j=1}^{N}\mathbf{T}_j^T\mathbf{I}_j\mathbf{T}_j \tag{17}$$

is the total inertia matrix of flexible substructures,

$$\mathbf{A} = \sum_{j=1}^{N}\mathbf{T}_j^T\mathbf{A}_j\mathbf{P}_j \tag{18}$$

is the total coupling matrix for the rotational displacements of the rigid main body and the displacements of flexible substructures,

$$\mathbf{W} = \sum_{j=1}^{N} \mathbf{T}_j^T \mathbf{W}_j \mathbf{P}_j \tag{19}$$

is the total coupling matrix for the translational displacements of the rigid main body and the displacements of flexible substructures, and

$$\mathbf{Q}_a = \sum_{j=1}^{N} \mathbf{T}_j^T \mathbf{Q}_j \mathbf{T}_j \tag{20}$$

is the total coupling matrix for the translational and rotational displacements of the rigid main body, while

$$\mathbf{M}_j = \int_{m_j} \mathbf{C}_j^T \mathbf{C}_j dm, \tag{21}$$

$$\mathbf{I}_j = \int_{m_j} ({}^l\tilde{\mathbf{r}}_{b,o} + {}^l\tilde{\mathbf{r}}_{o,p_0})^T ({}^l\tilde{\mathbf{r}}_{b,o} + {}^l\tilde{\mathbf{r}}_{o,p_0}) dm, \tag{22}$$

$$\mathbf{A}_j = {}^l\tilde{\mathbf{r}}_{b,o}\mathbf{W}_j + \int_{m_j} {}^l\tilde{\mathbf{r}}_{o,p_0}\mathbf{C}_j dm, \tag{23}$$

$$\mathbf{W}_j = \int_{m_j} \mathbf{C}_j dm, \tag{24}$$

$$\mathbf{Q}_j = \int_{m_j} ({}^l\tilde{\mathbf{r}}_{b,o} + {}^l\tilde{\mathbf{r}}_{o,p_0})^T dm. \tag{25}$$

$\mathbf{T}_j$ is $\mathbf{T}_{b,l}$ for the jth element, and $\mathbf{P}_j$ is the assembling matrix relating the jth element displacement vector $\mathbf{d}_j$ and the displacement vector of total flexible substructures $\mathbf{d}$ as expressed in the following form:

$$\mathbf{d}_j = \mathbf{P}_j \mathbf{d} \tag{26}$$

2.1.2. Potential energy

The potential energy of the satellite consists of the potential energy of its undeformed state and the potential energy due to elastic deformations of flexible substructures. The potential energy of the undeformed state, in this research, is measured relative to the earth.

$$E_{pr} = E_{pr}(\mathbf{r}_{e,b}), \tag{27}$$

where $\mathbf{r}_{e,b} = \mathbf{r}_{e,i} + \mathbf{r}_{i,b}$, $\mathbf{r}_{e,i}$ is a vector from centre of the earth to O_i. If the satellite orbit is circular, $\mathbf{r}_{e,i}$ is constant, so

$$E_{pr} = E_{pr}(\mathbf{r}_{i,b}). \tag{28}$$

The potential energy due to elastic deformations is the sum of strain energy of flexible substructures and the potential energy due to external forces acting on the substructures with minus sign. The potential energy of element j ($j = 1, 2, ..., N$) in the flexible substructure can be written as [16]:

$$E_{pa_j} = \frac{1}{2}\int_{V_j} \boldsymbol{\sigma}_j^T \boldsymbol{\varepsilon}_j dV - \int_{V_j} {}^l\mathbf{r}_{p0,p}^T \mathbf{F}_f dV, \tag{29}$$

where $\boldsymbol{\sigma}_j$, $\boldsymbol{\varepsilon}_j$, and $\mathbf{F}_f$ are stress vector, strain vector, and distributed external forces vector at the element j. Again, by following the general finite element method procedures and employing Eq. (13), the total potential energy due to the elastic deformations of flexible substructures can be written in the following form:

$$E_{pa} = \frac{1}{2}\mathbf{d}^T \mathbf{K} d - \mathbf{d}^T \mathbf{F}_a, \tag{30}$$

where

$$\mathbf{K} = \sum_{j=1}^{N} \mathbf{P}_j^T \mathbf{K}_j \mathbf{P}_j \tag{31}$$

is the total stiffness matrix of flexible substructures, and

$$\mathbf{F}_a = \sum_{j=1}^{N} \mathbf{P}_j^T \mathbf{F}_j \tag{32}$$

is the total discrete external forces vector acting on all nodes of flexible substructures, while

$$\mathbf{F}_j = \int_{V_j} \mathbf{C}_j^T \mathbf{F}_f dV \tag{33}$$

is a discrete external forces acting on the nodes of element j,

$$\mathbf{K}_j = \int_{V_j} \mathbf{C}_j^T \mathbf{B}_j^T \mathbf{R}_j \mathbf{B}_j \mathbf{C}_j dV \tag{34}$$

is a stiffness matrix of element j, $\mathbf{B}_j$ is an operator matrix containing first or second order derivative operators, and $\mathbf{R}_j$ is an elasticity matrix of element j.

2.1.3. Lagrangian formulation

To derive the general equations of motion of a flexible spacecraft by using Lagrangian procedure, the Lagrangian operator

$$L = E_k - E_p = (E_{kb} + E_{ka}) - (E_{pr} + E_{pa}) \tag{35}$$

and the Lagrange's equation of motion

$$\frac{d}{dt}\left[\frac{\partial L}{\partial \dot{\mathbf{q}}}\right] - \frac{\partial L}{\partial \mathbf{q}} + \frac{\partial S}{\partial \dot{\mathbf{q}}} = \mathbf{F} \tag{36}$$

are used, where $\mathbf{q}$ is the displacements vector (which contains 3 translational and 3 rotational displacements of the rigid main body, and the displacements of flexible substructures), $\mathbf{F}$ is a

general external forces vector, and S is the Rayleigh's dissipation. The Rayleigh's dissipation is defined as

$$S = \frac{1}{2}\dot{\mathbf{q}}^T \mathbf{D}\dot{\mathbf{q}} \tag{37}$$

where $\mathbf{D}$ is a system damping matrix.

Then, it is assumed that control (external) forces acting on the rigid main body of the satellite are much larger than the forces resulting from the potential energy of the undeformed state. By using Eqs. (5), (14), (28), (30), (35), (36), and (37), the equations of motion of the satellite then can be written as follows:

$$m\ddot{\mathbf{r}} + \mathbf{Q}\dot{\boldsymbol{\omega}} + \mathbf{W}\ddot{\mathbf{d}} = \mathbf{F}_b - \mathbf{F}_b^*(\dot{\mathbf{r}}, \boldsymbol{\omega}, \dot{\mathbf{d}}) \tag{38}$$

$$\mathbf{Q}^T\ddot{\mathbf{r}} + \mathbf{I}\dot{\boldsymbol{\omega}} + \mathbf{A}\ddot{\mathbf{d}} = \mathbf{T}_b - \mathbf{T}_b^*(\dot{\mathbf{r}}, \boldsymbol{\omega}, \dot{\mathbf{d}}) \tag{39}$$

$$\mathbf{W}^T\ddot{\mathbf{r}} + \mathbf{A}^T\dot{\boldsymbol{\omega}} + \mathbf{M}\ddot{\mathbf{d}} + \mathbf{D}\dot{\mathbf{d}} + \mathbf{K}\mathbf{d} = \mathbf{F}_a - \mathbf{F}_a^*(\dot{\mathbf{r}}, \boldsymbol{\omega}, \dot{\mathbf{d}}) \tag{40}$$

where $\mathbf{r}$ and $\boldsymbol{\omega}$ replace the notations of $\mathbf{r}_{i,b}$ and $\boldsymbol{\omega}_{b,i}$, $\mathbf{F}_b$ and $\mathbf{T}_b$ are external forces and torques vectors acting on the rigid main body, $\mathbf{F}_a$ has been explained in Eq. (32), and

$$\mathbf{F}_b^*(\dot{\mathbf{r}}, \boldsymbol{\omega}, \dot{\mathbf{d}}) = \tilde{\boldsymbol{\omega}}(m\dot{\mathbf{r}} + \mathbf{Q}\boldsymbol{\omega} + \mathbf{W}\dot{\mathbf{d}}) \tag{41}$$

$$\mathbf{T}_b^*(\dot{\mathbf{r}}, \boldsymbol{\omega}, \dot{\mathbf{d}}) = \tilde{\boldsymbol{\omega}}(\mathbf{Q}^T\dot{\mathbf{r}} + \mathbf{I}\boldsymbol{\omega} + \mathbf{A}\dot{\mathbf{d}}) + \tilde{\dot{\mathbf{r}}}(m\dot{\mathbf{r}} + \mathbf{Q}\boldsymbol{\omega} + \mathbf{W}\dot{\mathbf{d}}) \tag{42}$$

$$\mathbf{F}_a^*(\dot{\mathbf{r}}, \boldsymbol{\omega}, \dot{\mathbf{d}}) = \mathbf{B}(\dot{\mathbf{r}}, \boldsymbol{\omega}, \dot{\mathbf{d}})(\mathbf{W}^T\dot{\mathbf{r}} + \mathbf{A}^T\boldsymbol{\omega} + \mathbf{M}\dot{\mathbf{d}}) \tag{43}$$

are nonlinear terms containing multiplications between components of $\dot{\mathbf{r}}$, $\boldsymbol{\omega}$, and $\dot{\mathbf{d}}$, while $\mathbf{B}(\dot{\mathbf{r}}, \boldsymbol{\omega}, \dot{\mathbf{d}})$ in Eq. (43) is the matrix with elements consisted of linear combinations between components of $\dot{\mathbf{r}}$, $\boldsymbol{\omega}$, and $\dot{\mathbf{d}}$, and the tilde ($\tilde{}$) means the skew-symmetric matrix of the specified vector. In many cases of observed spacecraft attitude dynamics, the values of the above nonlinear terms are small and can be neglected. This will result in linearized equations of motion of the flexible spacecraft. The linearized equations of motion will be used in the numerical simulations of this paper. For small Bryant's angles, they can be written in the matrix form as follows:

$$\begin{bmatrix} m\mathbf{U}_3 & \mathbf{Q} & \mathbf{W} \\ \mathbf{Q}^T & \mathbf{I} & \mathbf{A} \\ \mathbf{W}^T & \mathbf{A}^T & \mathbf{M} \end{bmatrix} \begin{Bmatrix} \ddot{\mathbf{r}} \\ \ddot{\boldsymbol{\Theta}} \\ \ddot{\mathbf{d}} \end{Bmatrix} + \begin{bmatrix} \mathbf{0}_{3\times3} & \mathbf{Q}\tilde{\boldsymbol{\omega}}_0 & \mathbf{0}_{3\times f} \\ \mathbf{0}_{3\times3} & \mathbf{I}\tilde{\boldsymbol{\omega}}_0 & \mathbf{0}_{3\times f} \\ \mathbf{0}_{f\times3} & \mathbf{A}^T\tilde{\boldsymbol{\omega}}_0 & \mathbf{D} \end{bmatrix} \begin{Bmatrix} \dot{\mathbf{r}} \\ \dot{\boldsymbol{\Theta}} \\ \dot{\mathbf{d}} \end{Bmatrix} + \begin{Bmatrix} \mathbf{0}_3 \\ \mathbf{0}_3 \\ \mathbf{K}\mathbf{d} \end{Bmatrix} = \begin{Bmatrix} \mathbf{F}_b \\ \mathbf{T}_b \\ \mathbf{F}_a \end{Bmatrix}, \tag{44}$$

where f is the total number of degrees of freedom of flexible substructures, $\tilde{\boldsymbol{\omega}}_0$ is the skew-symmetric matrix of angular velocity of the satellite orbit $\boldsymbol{\omega}_0$, and $\boldsymbol{\Theta}$ is a vector of Bryant's angles. In this paper, the flexible structural subsystems are supposed to have no dissipation properties, so that $\mathbf{D} = \mathbf{0}$.

2.2. A dynamic model of the satellite with solar panels modeled by rectangular plate elements

The mathematical formulation of a general spacecraft dynamic has been proposed in Eqs. (38–40). In this subsection, a particular model of a flexible spacecraft (a satellite consisted of a rigid main body carrying two symmetrical flexible solar panels) will be developed. To use Eqs. (38–40), the **W**, **A**, **M**, and **K** matrices need to be evaluated for a certain model of flexible substructures. In this study, the chosen attitude of the satellite as follows: the Z_b-axis of the main body-fixed frame points to the centre of earth, the Y_b-axis is normal to the orbital plane, and the X_b-axis points the velocity when there are no attitude errors.

For the application of finite element method to discretize elastic deformations of solar panels, the following assumptions are used:

1. The solar panels are divided into rectangular flat plate bending elements.
2. Each element has a constant mass density.
3. Only out-of-plane deformations of solar panels are considered.
4. External loads (both torques and forces) such as meteorite impacts on the solar panels are assumed to work on the nodal points of the elements.
5. The Y-axes of elements and the Y_b-axis of main body frame are parallel or antiparallel. The X-axes and Y-axes of elements are in the panel plane, and their Z-axes are normal to the plane.

Using the above assumptions, each element of solar panel has 12 degrees of freedom in total, as shown in Fig. 5.

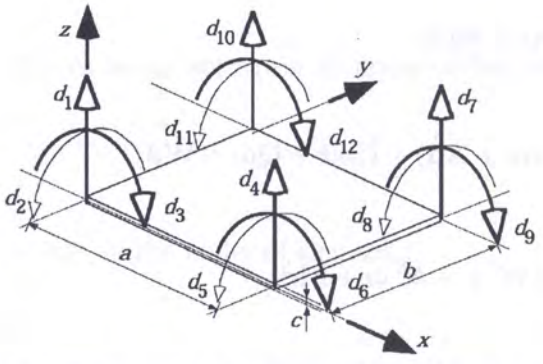

Fig. 5. A rectangular plate bending element model of solar panel

For an isotropic plate, the elasticity matrix $\mathbf{R}_j$ used in Eq. (34) can be written as

$$\mathbf{R}_j = \frac{Ec^3}{12(1-\nu^2)} \begin{bmatrix} 1 & \nu & 0 \\ \nu & 1 & 0 \\ 0 & 0 & \dfrac{1-\nu}{2} \end{bmatrix}, \tag{45}$$

where E, c (see Fig. 5), and ν are the Young's modulus, thickness, and Poisson's ratio of jth element respectively.

The shape function matrix introduced by Bogner [1] is selected. This shape function matrix can guarantee that deflections and slopes are all continuous on the edges of elements, and its expression for the jth element is as follows:

$$\mathbf{C}_j^T = \begin{bmatrix} (1+2\xi)(1-\xi)^2(1+2\eta)(1-\eta)^2 \\ (1+2\xi)(1-\xi)^2\eta(1-\eta)^2 b \\ -\xi(1-\xi)^2(1+2\eta)(1-\eta)^2 a \\ (1+2\xi)(1-\xi)^2(3-2\eta)\eta^2 \\ -(1+2\xi)(1-\xi)^2(1-\eta)\eta^2 b \\ -\xi(1-\xi)^2(3-2\eta)\eta^2 a \\ (3-2\xi)\xi^2(3-2\eta)\eta^2 \\ -(3-2\xi)\xi^2(1-\eta)\eta^2 b \\ (1-\xi)\xi^2(3-2\eta)\eta^2 a \\ (3-2\xi)\xi^2(1+2\eta)(1-\eta)^2 \\ (3-2\xi)\xi^2\eta(1-\eta)^2 b \\ (1-\xi)\xi^2(1+2\eta)(1-\eta)^2 a \end{bmatrix}, \tag{46}$$

where a and b are the length and width of element respectively, $0 \leq (\xi = \frac{x}{a}) \leq 1$, and $0 \leq (\eta = \frac{y}{b}) \leq 1$ (see Fig. 5). For this shape function matrix, the coupling matrix $\mathbf{A}_j$ defined in Eq. (23) can be obtained as follows:

$$\mathbf{A}_j^T = \frac{\rho abc}{24} \begin{bmatrix} 6y_{0_j} + \frac{9}{5}b & -6x_{0_j} - \frac{9}{5}a & 0 \\ by_{0_j} + \frac{2}{5}b^2 & -bx_{0_j} - \frac{3}{10}ab & 0 \\ -ay_{0_j} - \frac{3}{10}ab & ax_{0_j} + \frac{2}{5}a^2 & 0 \\ 6y_{0_j} + \frac{21}{5}b & -6x_{0_j} - \frac{9}{5}a & 0 \\ -by_{0_j} - \frac{3}{5}b^2 & bx_{0_j} + \frac{3}{10}ab & 0 \\ -ay_{0_j} - \frac{7}{10}ab & ax_{0_j} + \frac{2}{5}a^2 & 0 \\ 6y_{0_j} + \frac{21}{5}b & -6x_{0_j} - \frac{21}{5}a & 0 \\ -by_{0_j} - \frac{3}{5}b^2 & bx_{0_j} + \frac{7}{10}ab & 0 \\ ay_{0_j} + \frac{7}{10}ab & -ax_{0_j} - \frac{3}{5}a^2 & 0 \\ 6y_{0_j} + \frac{9}{5}b & -6x_{0_j} - \frac{21}{5}a & 0 \\ by_{0_j} + \frac{2}{5}b^2 & -bx_{0_j} - \frac{7}{10}ab & 0 \\ ay_{0_j} + \frac{3}{10}ab & -ax_{0_j} - \frac{3}{5}a^2 & 0 \end{bmatrix}, \tag{47}$$

where x_{0_j} and y_{0_j} are the components of ${}^l\mathbf{r}_{b,o}$ for the jth element along its x_j and y_j-axes respectively (see Fig. (3), ρ is the mass density, while the inertia matrix $\mathbf{I}_j$ can be written as follows :

$$\mathbf{I}_j = \rho abc \begin{bmatrix} I_{j11} & I_{j21} & I_{j31} \\ I_{j21} & I_{j22} & I_{j32} \\ I_{j31} & I_{j32} & I_{j33} \end{bmatrix}, \tag{48}$$

where

$$I_{j11} = y_{0_j}^2 + \frac{1}{12}c^2 + \frac{1}{3}b^2 + y_{0_j}b,$$

$$I_{j21} = -\frac{1}{2}(\frac{1}{2}ab + y_{0_j}a + x_{0_j}b) - x_{0_j}y_{0_j},$$

$$I_{j31} = I_{j32} = 0,$$

$$I_{j22} = x_{0_j}^2 + \frac{1}{12}c^2 + \frac{1}{3}a^2 + x_{0_j}a,$$

$$I_{j33} = x_{0_j}^2 + y_{0_j}^2 + \frac{1}{3}(a^2 + b^2) + x_{0_j}a + y_{0_j}b,$$

and the coupling matrix for rotational displacements of the main body and the displacements of jth element can be written as follows:

$$\mathbf{W}_j = \frac{\rho abc}{24} \begin{bmatrix} 0 & 0 & 0 & 0 & 0 & 0 & 0 & 0 & 0 & 0 & 0 & 0 \\ 0 & 0 & 0 & 0 & 0 & 0 & 0 & 0 & 0 & 0 & 0 & 0 \\ 6 & b & -a & 6 & -b & -a & 6 & -b & a & 6 & b & a \end{bmatrix} \tag{49}$$

3. Rest-to-rest roll maneuver of a flexible satellite under bang-bang roll torque input

Since time is the independent variable, if the initial values of dependent variables are given in addition to the boundary conditions, the dynamics of the modelled satellite can be simulated numerically by solving the set of differential equations of motion, Eqs. (44). In this study, the observed satellite is supposed to has no control on the flexible solar panels. The control inputs are applied on the rigid main body only, either forces or torques at the center of mass of satellite, as on-off reaction jets with constant amplitude force pulses. For such system, when the working control commands are only the torque inputs, the resulted attitude angle acceleration of satellite as a rigid body motion can be written as

$$\begin{Bmatrix} \ddot{\phi} \\ \ddot{\theta} \\ \ddot{\psi} \end{Bmatrix} = \begin{bmatrix} I_x & I_{xy} & I_{xz} \\ I_{xy} & I_y & I_{yz} \\ I_{xz} & I_{yz} & I_z \end{bmatrix}^{-1} \begin{Bmatrix} T_{b_x}(t) \\ T_{b_y}(t) \\ T_{b_z}(t) \end{Bmatrix}, \tag{50}$$

where I_x, I_y, I_z, I_{xy}, I_{xz}, and I_{yz} are components of inertia matrix of the whole satellite, $\mathbf{I}$, T_{b_x}, T_{b_y}, and T_{b_z} are components of the torque $\mathbf{T}_b$ along X_b, Y_b, and Z_b-axes respectively, depending on time t. By integrating Eq. (50) with respect to time we get an expression of desired attitude angle velocity,

$$\begin{Bmatrix} \dot{\phi}_d \\ \dot{\theta}_d \\ \dot{\psi}_d \end{Bmatrix} = \int \begin{bmatrix} I_x & I_{xy} & I_{xz} \\ I_{xy} & I_y & I_{yz} \\ I_{xz} & I_{yz} & I_z \end{bmatrix}^{-1} \begin{Bmatrix} T_{b_x}(t) \\ T_{b_y}(t) \\ T_{b_z}(t) \end{Bmatrix} dt \tag{51}$$

and integrating once more gives a desired attitude angle displacement,

$$\begin{Bmatrix} \phi_d \\ \theta_d \\ \psi_d \end{Bmatrix} = \int\int \begin{bmatrix} I_x & I_{xy} & I_{xz} \\ I_{xy} & I_y & I_{yz} \\ I_{xz} & I_{yz} & I_z \end{bmatrix}^{-1} \begin{Bmatrix} T_{b_x}(t) \\ T_{b_y}(t) \\ T_{b_z}(t) \end{Bmatrix} dt\, dt. \tag{52}$$

The main body of a real satellite consists of electronics, fuel, units of communication, data acquisition and control, power system, and so on. It is useful to model the main body as a collection of lumped masses at certain positions from the origin of main body-fixed frame O_b since the locations of O_b and mass center of the whole modelled satellite are permitted to be at the different points. By using a number of lumped masses, the inertia matrix $\mathbf{I}_b$ and coupling matrix $\mathbf{Q}_b$ of the main body can be calculated simply. In this simulation, the main body of satellite is modeled by 6 lumped masses at certain positions indicated in Table 1, and the parameters of flexible solar panels being used can be seen in Table 2.

Table 1. Lumped masses consisting of the main body

Mass (kg)	Position (m)		
	x_b	y_b	z_b
400	0.40	0.00	0.00
400	-0.40	0.00	0.00
500	0.00	0.50	0.00
500	0.00	-0.50	0.00
550	0.00	0.00	1.40
550	0.00	0.00	-1.40

Table 2. Parameters of the solar panels of satellite

Description	Values
Number of solar panels	2
Dimension of each solar panel (m^3)	$12 \times 2.4 \times 0.03$
Young's modulus, E (N/m^2)	0.6×10^8
Poisson ratio ν	0.3
Mass density, ρ (kg/m^3)	120
Number of elements in each solar panel	16
Dimension of each element, $b \times a \times c$ (m^3)	$1.5 \times 1.2 \times 0.03$
Offset angle, δ (degrees)	0
Distance between panel's root and O_b (m)	1.80

The offset angle of solar panels δ is taken to be 0^o. However, for this configuration, the origin of rigid main body fixed reference frame coincide with the centre of mass of the whole satellite in the undeformed state (i.e. $\mathbf{Q}_b = \mathbf{0}$), I_x = 17,510 kg-m2, I_y = 2,384 kg-m2, I_z = 15,582 kg-m2, and $I_{xy} = I_{xz} = I_{yz} = 0$. The initial condition of the satellite is given to be undeformed state; the main body fixed frame and the orbital reference frame coincide with the inertial reference frame. The orbital frame moves relative to the inertial frame with constant angular velocity

$$\boldsymbol{\omega}_o = -\omega_o \boldsymbol{j}_i, \tag{53}$$

where $\boldsymbol{j}_i$ is the unit vector in Y_i-axis direction, ω_o = 7.29 10-5 rad/sec, so that F_o performs in F_i one rotation per sidereal day (24 hours of sidereal time or 23 hours 56 minutes 4.09054 seconds of mean solar time).

The roll angle of the satellite will be changed by applying a roll torque command to the desired angle 5°, i.e. about 0.0873 rad. The shortest duration time of constant-amplitude command for rest-to-rest slew maneuver is a bang-bang input. If the amplitude of command is determined to

be 20 N-m, constraint equations that must be satisfied for this rest-to-rest slew maneuver are: $\{\dot{\phi}_d, \dot{\theta}_d, \dot{\psi}_d\}^T = \{0, 0, 0\}^T$ in Eq. (51), $\{\phi_d, \theta_d, \psi_d\}^T = \{0.0873, 0, 0\}^T$ in Eq. (52), and T_{b_x} in the both equations equals to 20 if $0 < t \leq t_{bb_s}$ and -20 if $t_{bb_s} < t \leq t_{bb_l}$, where t_{bb_s} and t_{bb_l} are the switching time and length of bang-bang respectively. The resulted profile of roll bang-bang torque needed for the maneuver can be seen in Fig. 6(a).

Under this input, the roll angle attitude will change, while pitch and yaw angle are not excited. The roll angle changes to the desired displacement, but after roll maneuver input was stopped, the roll angle still oscillates with a very large amplitude dominantly at the period about 18.68 seconds, i.e. at the natural frequency 0.3364 rad/sec. The amplitude of residual oscillation of roll angle reaches until 0.156 rad, or 8.94°, as shown in Fig. 6(b), or about 179% of the desired roll displacement. Of course such residual oscillation is very unacceptable and may disturb the mission of a satellite. The largest deflections on solar panels take place at their tips. The node 25, shown in Fig. 6(c), experiences unlikely local vertical vibration with high deflection amplitude of 3.219 meters. Compared with solar panel's length of 12 m, this deflection is about 27%, a condition where the use of local reference frame for its element in finite element method fixed at its initial condition is no longer true.

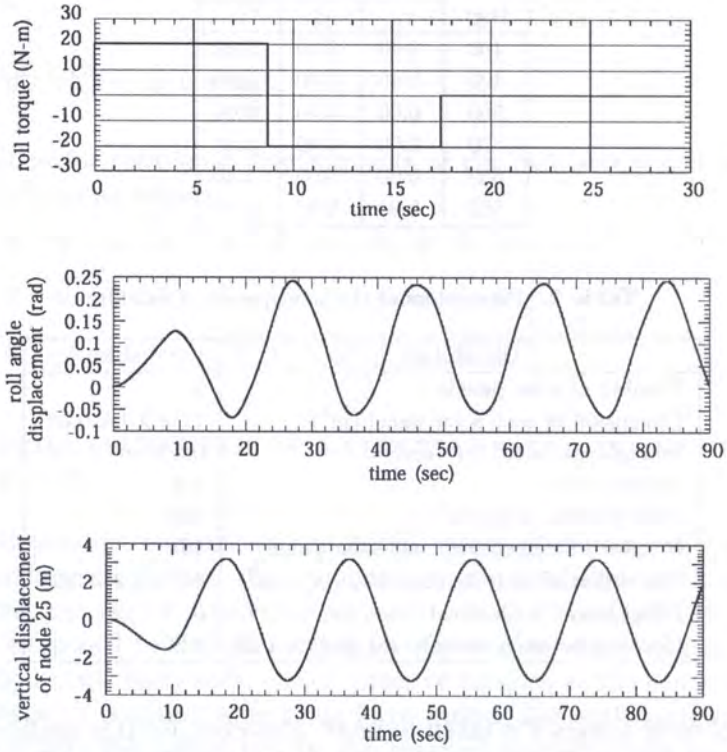

Fig. 6. (a) Bang-bang roll torque input for the length of 17.486 sec. (b) Roll motion of the satellite under the bang-bang roll torque input. (c) Vertical deflection of node 25 of solar panel in local reference frame under the bang-bang roll torque input

4. Input Shaper to Reduce Residual Vibration in Rest-to-Rest Slew Maneuvers

The flexible satellite studied here is equipped with on-off reaction jets, so it cannot produce variable amplitude actuation force; the satellite must be controlled by constant amplitude force pulses. For this kind of satellite, when the bang-bang input was used for rest-to-rest slew maneuvers, the residual vibration of flexible members and attitude oscillation of rigid main body after slewing

maneuver input was removed can be relatively large enough compared with the desired new attitude. By shaping the input, the residual vibration can be reduced.

The inputs to the system under consideration must consist only of positive or negative constant-amplitude force pulses. For rest-to-rest slews, the commands must contain both positive and negative pulses so that the system can be accelerated and then decelerated back to zero velocity. A series of alternating-sign pulses for rest-to-rest time optimal slew maneuver can be generated by convolving a step with an input shaper of the form

$$\begin{bmatrix} A_i \\ t_i \end{bmatrix} = \begin{bmatrix} 1 & -2 & 2 & -2 & \dots & -2 & 1 \\ 0 & t_2 & t_3 & t_4 & \dots & t_{n_{\text{odd}}-1} & t_{n_{\text{odd}}} \end{bmatrix}, \tag{54}$$

where $i = 1, \dots, n_{\text{odd}}$, A_i is the amplitude of the ith impulse, t_i is the time location of the ith impulse, and n_{odd} is odd, or

$$\begin{bmatrix} A_i \\ t_i \end{bmatrix} = \begin{bmatrix} 1 & -2 & 2 & -2 & \dots & 2 & -1 \\ 0 & t_2 & t_3 & t_4 & \dots & t_{n_{\text{even}}-1} & t_{n_{\text{even}}} \end{bmatrix}, \tag{55}$$

where $i = 1, \dots, n_{\text{even}}$, and n_{even} is an even integer.

Figure 7 demonstrates Eq. (54), that a step convolved with this type of an input shaper results in a series of alternating sign, variable-width pulses. Equations (54) and (55) lead to our first constraint equations for rest-to-rest shapers:

$$\begin{cases} A_i = 1 & i = 1, n_{\text{odd}} \\ A_i = 2(-1)^{(i-1)} & i = 2, 3, \dots, (n_{\text{odd}} - 1) \end{cases} \tag{56}$$

or

$$\begin{cases} A_i = 1 & i = 1 \\ A_i = -1 & i = n_{\text{even}} \\ A_i = 2(-1)^{(i-1)} & i = 2, 3, \dots, (n_{\text{even}} - 1) \end{cases} \tag{57}$$

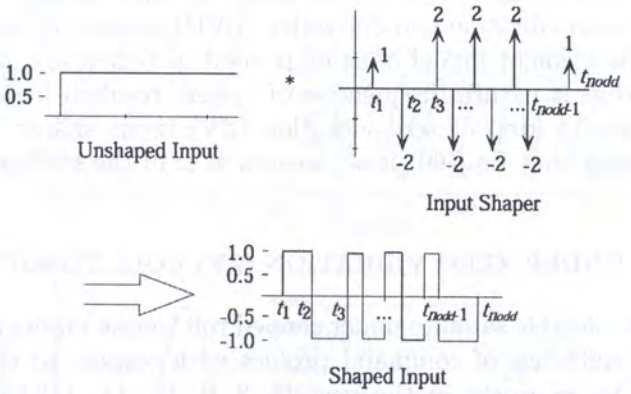

Fig. 7. Input shaping to generate a series of alternating-sign pulses

The next constraint equations must ensure that the system will move the desired amount. For the system under only roll torque input as studied in this paper, these equations governed by Eqs. (51) and (52) of the previous section, set the roll maneuver of rigid-body motion; however, the main purpose of input shaping is to limit the amount of residual vibration that occurs when the system reaches its desired setpoint. The constraint equation limiting vibration amplitude can be formulated

as a ratio of residual vibration amplitude with input shaping divided by residual vibration without shaping. When the techniques are designed for use with on-off actuators, it would be appropriate to use a baseline input. Whenever possible, the bang-bang input is used as the standard for commands that slew from rest to rest.

A bang-bang input can be viewed as a step input convolved with a shaper of the form

$$\begin{bmatrix} A_i \\ t_i \end{bmatrix} = \begin{bmatrix} 1 & -2 & 1 \\ 0 & t_{bb_s} & t_{bb_l} \end{bmatrix} \tag{58}$$

where t_{bb_s} is the switching time and t_{bb_l} is the length of the bang-bang. This is demonstrated by the first three impulses in Fig. 7 if the value of the third impulse is changed from 2 to 1.

The amplitude of residual vibration of an undamped second-order system when subjected to a sequence of impulses can be expressed as a summation of the responses to individual impulses that is given in the reference [2]. The expression giving the amplitude is

$$R_{\text{amp}} = \sqrt{\left[\sum A_i \sin(\omega t_i)\right]^2 + \left[\sum A_i \cos(\omega t_i)\right]^2}, \tag{59}$$

where ω is the undamped natural frequency. We can construct the ratio of shaped to unshaped vibration by dividing Eq. (56) or (57) for the input shaper by the equivalent Eq. (59) for the impulse sequence corresponding to the unshaped input. The percentage vibration relative to a bang-bang is

$$V = \sqrt{\frac{[\sum A_i \sin(\omega t_i)]^2 + [\sum A_i \cos(\omega t_i)]^2}{\left[\sum A_{bb_j} \sin(\omega t_{bb_j})\right]^2 + \left[\sum A_{bb_j} \cos(\omega t_{bb_j})\right]^2}} \tag{60}$$

where A_{bb_j} and t_{bb_j} describe the input shaper corresponding to the bang-bang and are given by Eq. (58).

By including Eq. (60) in our set of constraint equations, we can set the level of vibration to the quantity V when the system's frequency is exactly ω. For example, when $V = 0.05$, the shaped vibration amplitude is 5% of the baseline vibration amplitude. However, the amount of frequencies of satellite studied in this paper is very large, varies from 1.078×10^{-15} rad/sec (or 1.717×10^{-16} Hz) until 343.4 rad/sec (or 54.65 Hz), then there may exist a large amount of residual vibration. For systems containing modelling errors, several kinds of input shaper have been proposed by researchers, for example zero vibration and derivative (ZVD) shaper [10] and extra-insensitive (EI) shaper [11]. For the finite element model of satellite used in this study, it is supposed that there is no modelling errors, that is natural frequencies of system resulted from calculation are in true values. Then, in such case, a kind of zero vibration (ZV) input shaper is chosen to reduce the residual vibration. It means that Eq. (60) is set to zero at ω of the strongest residual vibration.

5. Roll maneuver under zero vibration (ZV) roll torque input shaper

The roll maneuvers of the flexible satellite under shaped roll torque inputs are studied in this paper in order to observe the influence of command profiles with respect to the maximum deflections of flexible members. A lot of works in the past [7, 8, 9, 10, 11, 13] focused on the capability of shaped inputs to reduce the residual vibration, either investigating frequencies of system with errors or without errors in modelling. They usually minimized the time duration of command as one of constraint equations. However, in the attitude maneuvers of flexible system, the deflections of flexible members during maneuver under such shaped input can be very large and surpass the validity of the model being used. For simple models having one flexible mode and a rigid-body mode as studied by Singhose, Banerjee, and Seering [12], the expressions for the deflection of flexible one can be derived easily. But for the finite element model of satellite with flexible solar

panels studied here, where the system has a lot of flexible modes, the derivation of expressions for flexible member's deflections becomes very troublesome. The influence of command profiles with respect to the maximum flexible member's deflections is studied in this paper by using the results of computer simulations.

For the model described in the Sec. 3, and seeing Fig. 6, we knew that the strongest residual roll oscillation happens at $\omega = 0.3364$ rad/sec. With ZV input shaper with the same constant-amplitude roll torque input of 20 N-m, the percentage of vibration of Eq. (60) at this value of ω is set to zero. The minimum number of impulse for this kind of input shaper is 4, but it gives only one command profile where the resulted maximum deflection of flexible solar panels maybe surpassing the validity of model. In this study, the number of impulse compared is chosen from 4 until 6 in the time duration of command less than 40 seconds. The selected profiles can be seen in Table 3. For all cases in Table 3, results of simulation show that the maximum deflections of solar panels happen at their tip, and as representation, time responses of node 25 are given in this paper.

Table 3. Time Location of Impulses for Shaping the Roll Torque Inputs

Case number	Number of impulses	t_1 (sec)	t_2 (sec)	t_3 (sec)	t_4 (sec)	t_5 (sec)	t_6 (sec)
Case 1	4	0	11.391	30.069	37.356		
Case 2	5	0	6.314	10.806	15.298	21.612	
Case 3	5	0	0.055	7.402	26.076	37.464	
Case 4	6	0	8.266	14.024	17.061	26.649	30.692

Time responses for Case 1, where the input shaper consisted of four impulses with $t_4 = 37.356$ seconds, are plotted in Fig. 8. The resulted maximum roll displacement during the maneuver is 0.1957 rad (i.e. 11.23°) at $t = 28.916$ seconds as shown in Fig. 8(a), and the strongest residual oscillation after the input was removed happens at period 5.8 seconds with amplitude less than 0.0038 rad (i.e. 0.22°). In Fig. 8(b), we can see that the maximum deflection of node 25 is 3.125 meters at $t = 20.032$ seconds, while the strong residual vibration of this node occurs at periods of 2.31 and 18.67 seconds with total amplitude of 8.2 mm.

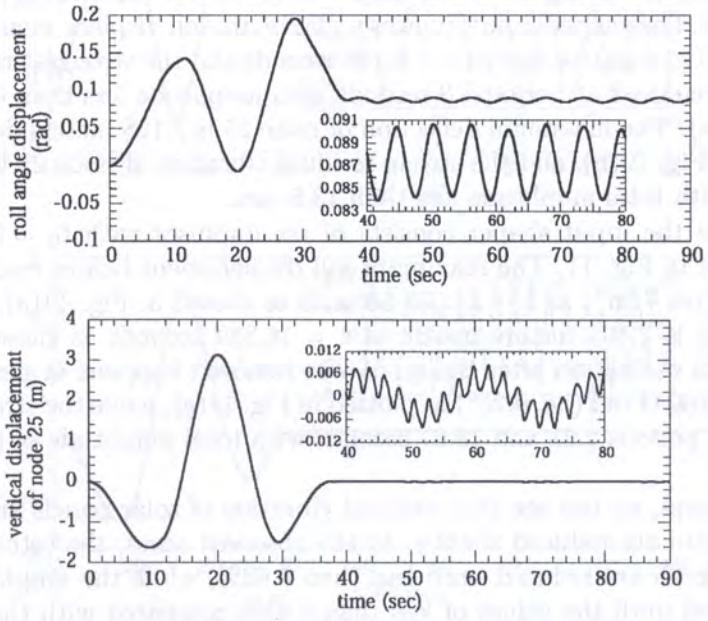

Fig. 8. Time responses of Case 1: (a) Roll motion of the satellite, and (b) Vertical deflection of node 25 of solar panel in local reference frame

For Case 2 where the input shaper consists of five impulses with $t_5 = 21.612$ seconds, time responses are plotted in Fig. 9. Under this input, the maximum roll displacement during the maneuver is 0.0937 rad (i.e. 5.37°) at $t = 7.648$ seconds as shown in Fig. 9(a) and the strongest residual roll oscillation happens at period 5.8 seconds with amplitude less than 0.0042 rad (i.e. 0.24°). The maximum deflection of node 25 is 1.347 meters at $t = 14.336$ seconds, while the strong residual vibration of this node occurs at periods 2.31 and 18.67 seconds with total amplitude less than 9.3 mm, as shown in Fig. 9(b).

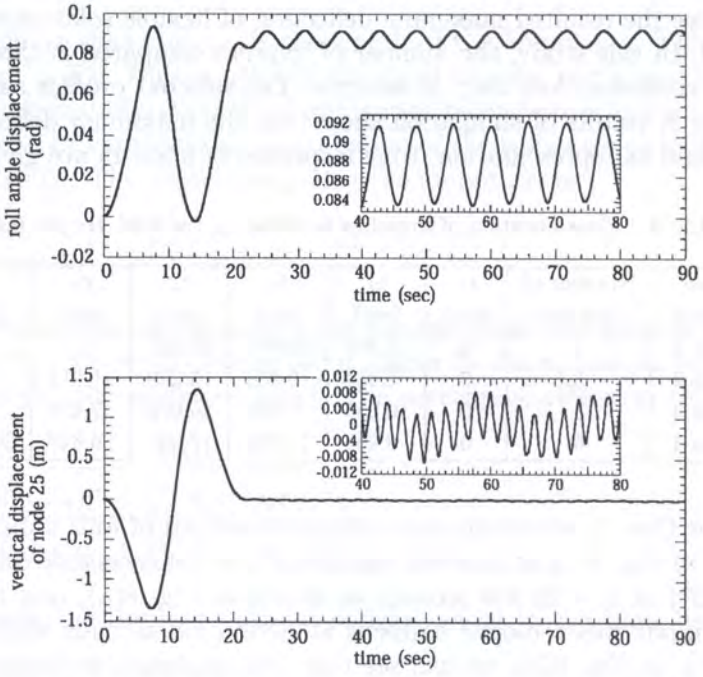

Fig. 9. Time responses of Case 2: (a) Roll motion of the satellite, and (b) Vertical deflection of node 25 of solar panel in local reference frame

For the input shaper consisting of five impulses with $t_5 = 37.464$ seconds in Case 3, time responses are plotted in Fig. 10. The shaped input induces a maximum roll displacement during the maneuver 0.1093 rad (i.e. 6.26°) in negative sign at $t = 8.448$ seconds and the strongest residual roll oscillation after the input was removed at period 5.8 seconds with amplitude less than 0.0038 rad (i.e. 0.22°) as shown in Fig. 10(a). The maximum deflection of node 25 is 3.128 meters downside at $t = 17.472$ seconds as shown in Fig. 10(b), and the strong residual vibration of node 25 is seen at periods 2.31 and 18.67 seconds with total amplitude less than 13.5 mm.

For Case 4 where the input shaper consists of six impulses with $t_6 = 30.692$ seconds, time responses are plotted in Fig. 11. The maximum roll displacement before reaching the new resting value is 0.1393 rad (i.e. 7.98°) at $t = 24.608$ seconds as shown in Fig. 11(a), while the maximum deflection of node 25 is 2.404 meters upside at $t = 16.389$ seconds as shown in Fig. 11(b). The strongest residual roll oscillation after the input was removed happens at period 5.8 seconds with amplitude less than 0.0044 rad (i.e. 0.25°) as plotted in Fig. 11(a), while the strong residual vibration of node 25 is seen at periods 2.31 and 18.67 seconds with total amplitude of 19.5 mm, as shown in Fig. 11(b).

From the above cases, we can see that residual vibration of solar panels and residual oscillation of roll angle of satellite are reduced slightly. In the observed cases, the total amplitudes of residual vibration of node 25 are reduced until less than 0.62%, while the amplitudes of residual roll oscillation are reduced until the values of less than 5.45% compared with the result of bang-bang input. Although the resulted residual vibrations under shaped inputs are good, the inputs in real application must be selected because the maximum deflection of solar panels during slew maneuver

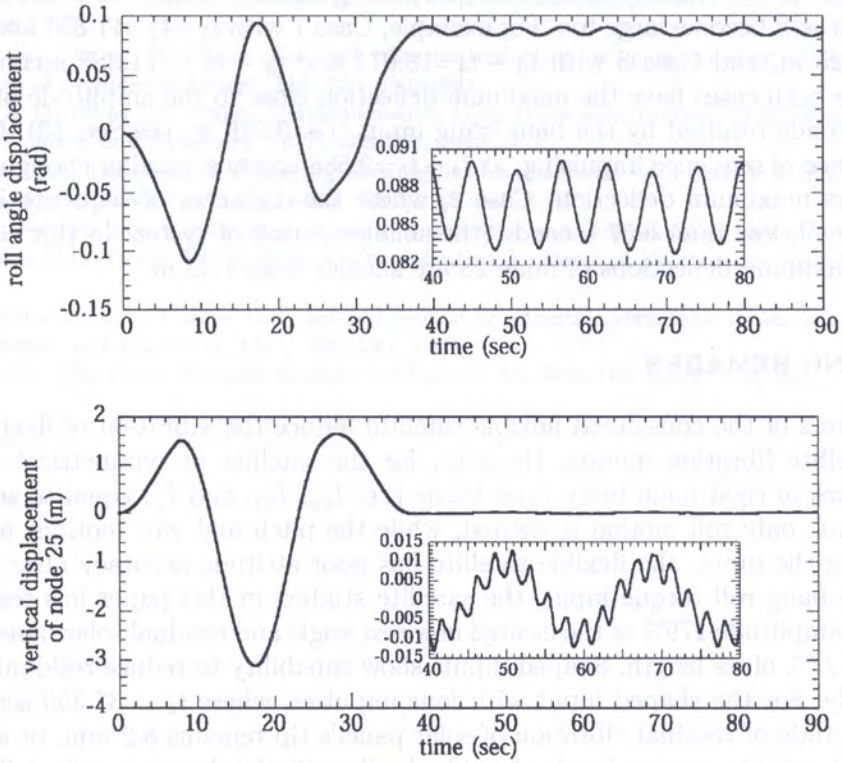

Fig. 10. Time responses of Case 3: (a) Roll motion of the satellite, and (b) Vertical deflection of node 25 of solar panel in local reference frame

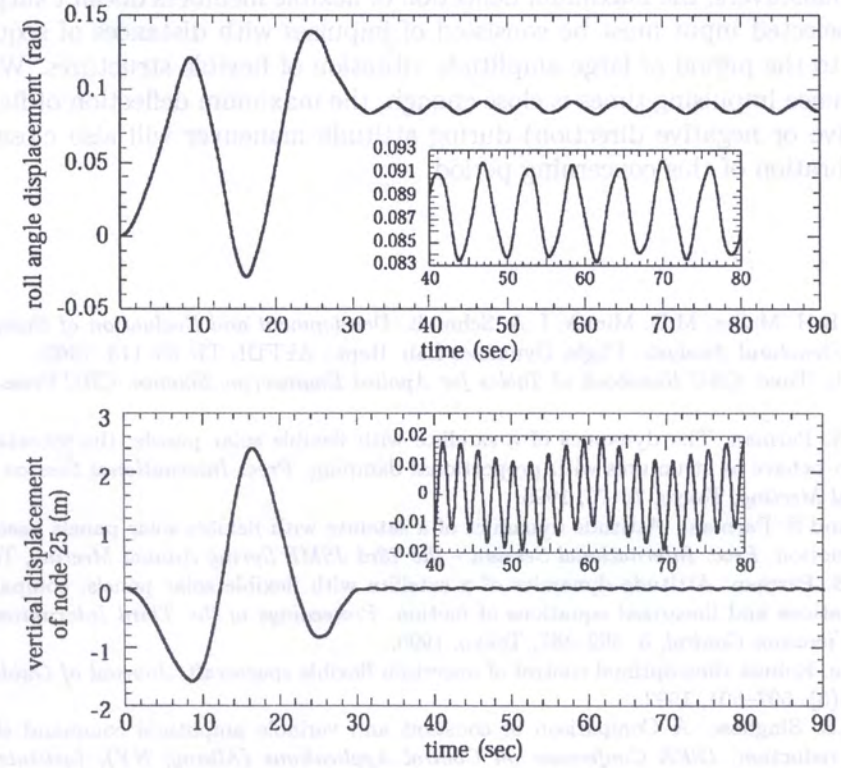

Fig. 11. Time responses of Case 5: (a) Roll motion of the satellite, and (b) Vertical deflection of node 25 of solar panel in local reference frame

can be very large. If the distance of sequence impulsing times is large, the deflection of structure during maneuver will become large too. For example, Case 1 with $t_1 - t_2$=11.391 and $t_2 - t_3$=18.678 seconds has 3.125 m, and Case 3 with $t_3 - t_4$=18.674 and $t_4 - t_5 = 11.388$ seconds has 3.128 m (downside). The both cases have the maximum deflection close to the amplitude of vibration with period 18.67 seconds resulted by the bang-bang input (i.e. 3.219 m, see Sec. (3). Case 4 with the maximum distance of sequence impulsing, at $t_4 - t_5$=9.588 seconds, smaller enough than 18.67 sec, has 2.404 meters maximum deflection. Case 2, where the distances of sequence impulsing times are relatively small, less than 6.57 seconds (the smaller period of system in this study after 18.67 seconds), the maximum deflections of node 25 are smaller than 1.35 m.

6. Concluding remarks

Slewing maneuvers of the considered flexible satellite induce the vibration of flexible members as well as the satellite libration motion. However, for the satellite in symmetrical conditions with respect to all axes of rigid main body fixed frame (i.e. I_{xy}, I_{xz}, and I_{yz} equal to zeros), under the roll torque inputs, only roll motion is excited, while the pitch and yaw motions are not induced. Without shaping the input, the flexible satellite has poor attitude accuracy after slew maneuver. Under the bang-bang roll torque input, the satellite studied in this paper has residual roll angle oscillation with amplitude 179% of the desired new rest angle and residual solar panel's tip vibration with amplitude 27% of its length. Shaped inputs show capability to reduce residual oscillation and vibration slightly. For the shaped input with four impulses, where $t_4 = 37.356$ sec of Case 1, the maximum amplitude of residual vibration of solar panel's tip remains 8.2 mm, or about 0.068% of its length, and the maximum amplitude of residual roll oscillation becomes only 4.4% of the desired angle displacement.

Although shaped inputs reduce successfully the residual oscillation of satellite attitude and residual vibration of flexible members, the input profile to be applied needs to be selected, so that during slewing maneuvers, the maximum deflection of flexible members doesn't surpass the validity of model. The selected input must be consisted of impulses with distances of sequence impulsing times not close to the period of large amplitude vibration of flexible structures. When the longest distance of sequence impulsing times is close enough, the maximum deflection of flexible structures (either in positive or negative direction) during attitude maneuver will also close enough to the amplitude of vibration of this concerning period.

References

[1] F.K. Bogner, R.H. Mallet, M.D. Minick, L.A. Schmidt. *Development and Evaluation of Energy Search Methods of Nonlinear Structural Analysis.* Flight Dynamics Lab. Rept., AFFDL TR 65–113, 1965.

[2] R.E. Bolz, G.L. Tuve. *CRC Handbook of Tables for Applied Engineering Science.* CRC Press, Boca Raton, FL, 1973.

[3] H. Koguchi, S. Parman. The dynamics of a satellite with flexible solar panels: the vibration of solar panels approached to behave as structures with proportional damping. *Proc. International Session – the 72nd JSME Spring Annual Meeting*, Tokyo, 70–73, 1995.

[4] H. Koguchi, and S. Parman. Attitude dynamics of a satellite with flexible solar panels based on its nonlinear equations of motion. *Proc. International Session – the 73rd JSME Spring Annual Meeting*, Tokyo, 75–78, 1996.

[5] H. Koguchi, S. Parman. Attitude dynamics of a satellite with flexible solar panels: comparison between the nonlinear equations and linearized equations of motion. *Proceedings of the Third International Conference on Motion and Vibration Control*, **3**: 382–387, Tokyo, 1996.

[6] Q. Liu, B. Wie. Robust time-optimal control of uncertain flexible spacecraft. *Journal of Guidance, Control, and Dynamics*, **15**(3): 597–604, 1992.

[7] L.Y. Pao, W.E. Singhose. A Comparison of constant and variable amplitude command shaping techniques for vibration reduction. *IEEE Conference on Control Applications (Albany, NY), Institute of Electrical and Electronics Engineers*, New York, 875–881, 1995.

[8] K. Rogers, W.P. Seering. Input shaping for limiting loads and vibration in systems with on-off actuators. *AIAA Guidance, Navigation, and Control Conf.*, San Diego, CA, 1996.

[9] T. Singh, S.R. Vadali. Robust time-optimal control: a frequency domain approach. *Journal of Guidance, Control, and Dynamics*, **17**(2): 346–353, 1994.

[10] W. Singhose, W. Seering, N. Singer. Residual vibration reduction using vector diagrams to generate shaped inputs. *Journal of Mechanical Design*, **116**: 654–659, 1994.

[11] W. Singhose, S. Derezinski, N. Singer. Extra-insensitive input shapers for controlling flexible spacecraft. *Journal of Guidance, Control, and Dynamics*, **19**(2): 385–391, 1996.

[12] W.E. Singhose, A.K. Banerjee, W.P. Seering. Slewing flexible spacecraft with deflection-limiting input shaping. *Journal of Guidance, Control, and Dynamics*, **20**(2): 291–298, 1997.

[13] C.J. Swiggert. Shaped torque techniques. *Journal of Guidance and Control*, **3**(5): 460–467, 1980.

[14] S. Thimoshenko, D.H. Young, W. Jr. Weaver. *The Vibration Problems in Engineering*. John Wiley & Sons, Inc., 1974.

[15] B. Wie, R. Sinha, Q. Liu., Robust time-optimal control of uncertain structural dynamic systems. *Journal of Guidance, Control, and Dynamics*, **15**(5): 980–983, 1993.

[16] O.C. Zienkiewicz. *The Finite Element Method*. 3rd Edition, McGraw-Hill Book Company, 1977.